10-10-2007

Sub-surface corrosion research on rock bolt system, perforated SS sheets and steel sets for the Yucca Mountain Repository — Quarterly technical report No. 13

Dhanesh Chandra
University of Nevada, Reno, dchandra@scs.unr.edu

Jaak J.K. Daemen
University of Nevada, Reno, daemen@mines.unr.edu

Sub-surface Corrosion Research on Rock Bolt System, Perforated SS Sheets and Steel Sets for the Yucca Mountain Repository

Quarterly Technical Report No. 13 (submitted during 4th Quarter of FY 2007)

Start Date of this Quarter, July 1, 2006 to September 30, 2007

Task No: ORD-FY04-019 and Document No: SIP-UNR-040

Prepared for U.S. DOE/UCCSN Cooperative Agreement Number DE-FC28-04RW12232

-submitted to-

United States Department of Energy
Office of Civilian Defense Radioactive Waste Management
Yucca Mountain Project
1551 Hillshire Drive, Suite A
Las Vegas NV 89134-6321

and

Harry Reid Center
University of Nevada, Las Vegas
4505 Maryland Parkway
Las Vegas Nevada 89154-4009

-submitted by-

Dhanesh Chandra, PI (Corrosion Team Leader)
and
Jaak Daemen (Co-PI)

Through
Chemical and Metallurgical Engineering Department
Metallurgical and Materials Engineering
Mail Stop 388
1664 N. Virginia Street
College of Engineering
University of Nevada, Reno
Reno NV 89557

October 10, 2007

DOE Technical Representative, Jaime Gonzalez and Raul Rebak, LLNL Lab. Partner
Quarterly Technical Progress Report
7/1/07 to 9/30/07

I. Statement of Work

The objective of this task is to conduct corrosion related research and predict the durability of SS-46, Mn-24, and AISI 4340 steel for Bernold shields or rock bolts. The importance of these results is that we have used the Yucca Mountain water chemistry (furnished by the DOE) as an electrolyte for conducting corrosion experiments on rock bolts and other materials. During this period, we used potentiodynamic and EIS tests to obtain corrosion rates. We present the results of potentiodynamic polarization for steels to identify potential corrosion inhibitors (SIP-UNR-040).

General Statements

Commonly available steels may be used to manufacture rock bolts used in underground applications such as tunnels for YM project. They are generally designed for high strength, but perhaps not so much emphasis is made on the corrosion aspects. We have performed corrosion tests on commercial rock bolts, such as AISI 4340 steel. This material may be potentially used for rock bolts of different types, and related materials for ground support of the repository. In this report No.13, corrosion rates were determined using potentiodynamic polarization method at different temperatures in different solutions using sodium bicarbonate and/or sodium silicate in both pure water and simulated seawater under deaerated conditions 25°C and 45°C.

Progress for the Period 7/1/07 to 9/30/07 on rock bolt materials

Subtask 1: Selection of New High-Strength Low-Alloy Steels, Stainless Steels for Rock Bolts, Steel Sets and Perforated Roof supports. In this report we show AISI 4340 steel results.

Subtask 2: Electrochemical tests to evaluate corrosion rate and possible corrosion mechanisms on AISI 4340 steel.

Subtask 6: Thermogravimetric (TGA) analysis of *Swellex* Mn-24, SS-46 steels and new work on Alloy 22 (just starting) for reliability tests at different temperatures - work in progress

II. Introduction

This report shows the work done for this period in accordance to cooperative agreement of University of Nevada system for the Task 019 *"Subsurface Corrosion Research on Rock Bolt System, Perforated SS Sheets and Steel Sets for the Yucca Mountain Repository"*, the overall objective of which is to conduct corrosion research and predict the durability of rock-bolts and other underground metallic roof supports. We are performing oxidation tests using Thermogravimetric Analyzer (TGA), and Potentiodynamic and immersion tests to determine the corrosion rates of rock bolts.

In this quarter:

- Potentiodynamic tests were performed to determine corrosion rates (CR) of 4340 Steel in pure water and simulated seawater using sodium bicarbonate and/or sodium silicate as electrolyte(s) at 25°C and 45°C under deaerated conditions.
- Oxidation studies were performed on *Swellex* Mn-24 and SS-46 steels using TGA to determine the oxidation kinetics of these steels at high temperatures - manuscript in preparation.

III. Results and Discussion

3.1 Corrosion Rates of AISI 4340 Steel

3.1.1 Introduction

Potentiodynamic scans of AISI 4340 steel were performed in solutions of sodium silicate (Na_2SiO_3) and/or sodium bicarbonate ($NaHCO_3$), in both pure water and simulated seawater (3.5 wt.% NaCl solution) at 25°C and 45°C under a continuous purge of nitrogen gas. These potentiodynamic tests build on the experiments presented in the previous quarterly report. Further tests at higher temperatures will be

performed to determine their passivity ranges in different solutions containing sodium silicate and/or sodium bicarbonate. Then, fresh electrochemical corrosion samples and immersion corrosion coupons will be soaked in these solutions for a period of time, immersed in Yucca Mountain solutions, and run using potentiodynamic polarization and immersion corrosion tests to determine their suitability as corrosion inhibitors for 4340 steel. These results can then be compared to the original amounts of silicate and bicarbonate already present in the naturally-occurring Yucca Mountain solution to determine their potential inhibition to corrosion and their associated long-term effects. Table 3.1.1 shows the individual chemicals of the Yucca Mountain solution that is currently being used to simulate conditions inside the repository, along with their equivalent weights and molarities, for reference.

Table 3.1.1. Simulated YM water composition for 1X concentration per Liter.

No.	CHEMICALS	Weight (mg/L)	Molarity (moles/L)
1	Magnesium sulfate ($MgSO_4 \cdot 7H_2O$)	50	2.03×10^{-4}
2	Magnesium chloride ($MgCl_2 \cdot 6H_2O$)	100	4.92×10^{-4}
3	Calcium chloride ($CaCl_2 \cdot 2H_2O$)	196	1.33×10^{-3}
4	Calcium sulfate ($CaSO_4 \cdot 2H_2O$)	210	1.22×10^{-3}
5	Potassium Bicarbonate ($KHCO_3$)	50	4.99×10^{-4}
6	Sodium Bicarbonate ($NaHCO_3$)	200	2.38×10^{-3}
7	Sodium Silicate ($Na_2SiO_3 \cdot 9H_2O$)	210	7.39×10^{-4}
8	Sodium Fluoride (NaF)	2	4.76×10^{-5}

3.1.2 Experimental

Electrochemical Tests

The electrochemical tests were performed using, quality-assured, commercially-available AISI 4340 steel. The chemical composition was analyzed by LTI[1] and is given in the 10th quarterly report. Disc-shaped test specimens approximately 0.25" thick were professionally cut and machined locally. The test specimens were mounted in epoxy with ~1.2 cm^2 surface area. An electrical connection wire was spot welded to the back of the steel specimen. Before the experiment, the sample was polished with 240 grit and 600 grit SiC emery papers and washed with deionized/distilled water before inserting them into the cell for electrochemical testing.

All the electrochemical experiments were conducted in a typical 1 liter Pyrex glass flask covered with a polytetrafluoroethylene lid (please see Quarterly report No. 5 for the photos and description of the apparatus). The reference electrode was a saturated silver/silver chloride (Ag/AgCl) electrode, which has a potential of 199mV more positive than the standard hydrogen potential. Continuously purged nitrogen gas in the sealed cell maintained constant pressure above the solution. A fritted glass capillary was used for continuous deaeration of the solution throughout the experiment at the rate of ~ 100 milliliters per minute (ml/min) using a flow meter. An electrically-heated water bath surrounded the test cell and maintained the temperature of the solution. The specimen was inserted into the electrolyte-filled cell and nitrogen was continuously purged for a minimum of 60 minutes, or until the steady-state open circuit potential was reached. The potentiodynamic tests were carried out at a scan rate of 0.2mV/sec using a commercially-available potentiostat.

All electrolyte solutions were prepared by mixing sodium silicate (Na_2SiO_3), sodium bicarbonate ($NaHCO_3$) and/or sodium chloride (NaCl) in distilled, de-ionized water at room temperature. After adding the salt(s) to the de-ionized water, the solution was stirred until fully dissolved. If any excess or undissolved salts precipitated out from the solution at the bottom of the flask, the solution was filtered before use. The pH of the solution was measured before and after each experimental run.[2]

The corrosion rate was calculated by following ASTM G59-97[3] and ASTM G102-89[4] procedures. During calculations, the polarization resistance (R_p) of the solution was neglected because it was shown by Yilmaz[5] that the electrolyte concentration was negligible. Tafel constants for both anodic and cathodic

reactions are assumed to be constant (0.12V/decade).[6] From the polarization resistance (R_p) value, the corrosion current density was calculated using equation 3.1, where K_1 = 3.27 x 10^{-3} mm·g/μA·cm·year, I_{corr} = μA/cm^2, ρ = 7.87 g/cm^3 and EW = 27.95 gm/equivalent.[4]

$$CR = K_1 \frac{I_{corr}}{\rho} EW \tag{3.1}$$

3.1.3 Results

Electrochemical Polarization & Passivity – 25°C

In this report, we show additional work on the passivation of AISI 4340 steel. Figures 3.1.1 – 3.1.4 show potentiodynamic scans of AISI 4340 steel at 25°C that were not presented in the last quarterly report, as well as Figures 3.1.5 & 3.1.6, which were revised to include a [0.01M Na_2SiO_3 + 0.1M $NaHCO_3$] scan for reference. Previously, only one scan containing [0.01M Na_2SiO_3 + 0.5M $NaHCO_3$] was presented in pure water and simulated seawater (3.5% NaCl). New experiments during this quarter were run to determine the effect of variation of SiO_3^{2-} with 0.5M & 0.1M HCO_3^- (in pure water and simulated seawater) on passivity, current density, corrosion rates, etc., to give a broader survey of the overall corrosion behavior. Tables 3.1.1 and 3.1.2 reflect the data obtained from these scans.

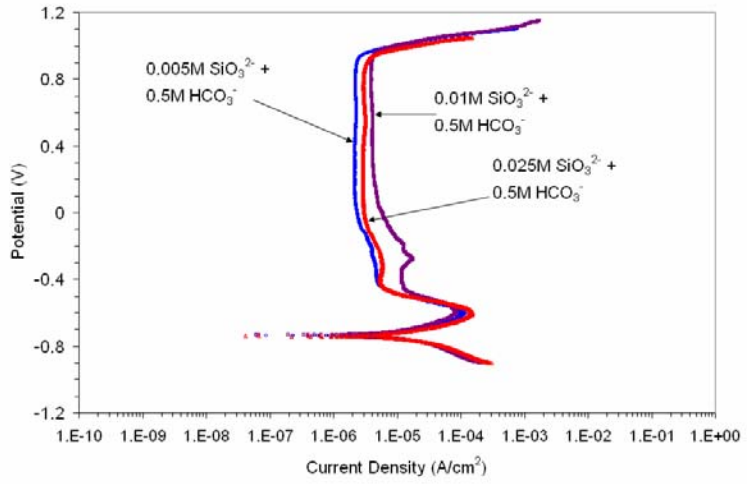

Figure 3.1.1. Potentiodynamic scans of AISI 4340 steel in deaerated, pure water solutions, with 0.5M $NaHCO_3$ and varying amounts of Na_2SiO_3 at 25°C.

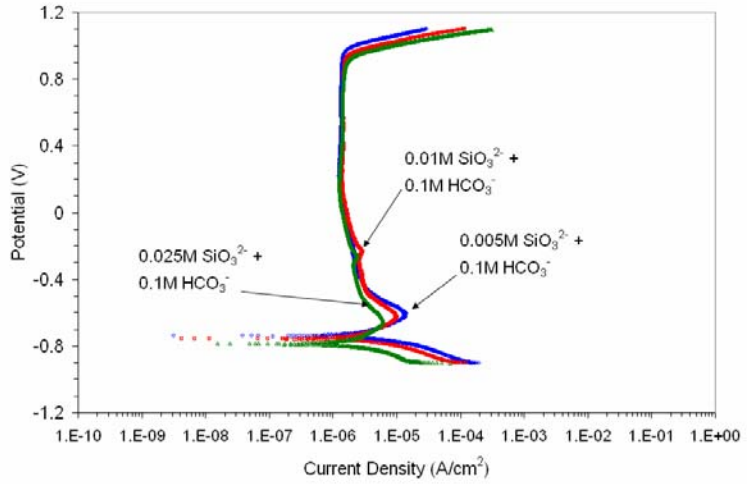

Figure 3.1.2. Potentiodynamic scans of AISI 4340 steel in deaerated, pure water solutions, with 0.1M $NaHCO_3$ and varying amounts of Na_2SiO_3 at 25°C.

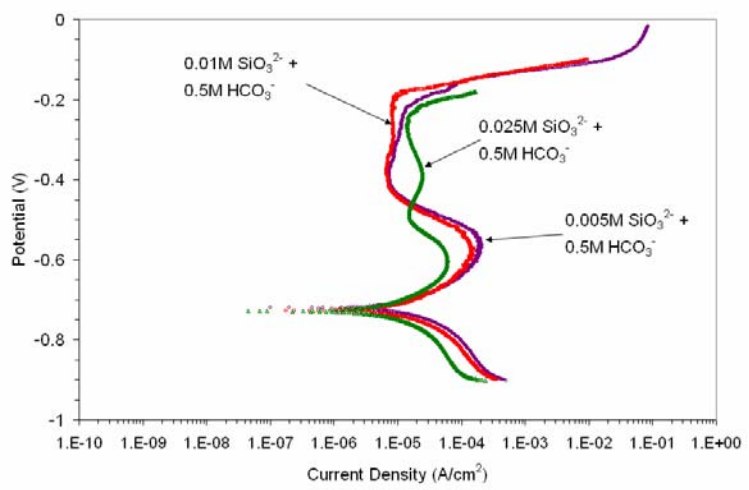

Figure 3.1.3. Potentiodynamic scans of AISI 4340 steel in deaerated, seawater solutions, with 0.5M $NaHCO_3$ and varying amounts of Na_2SiO_3 at 25°C.

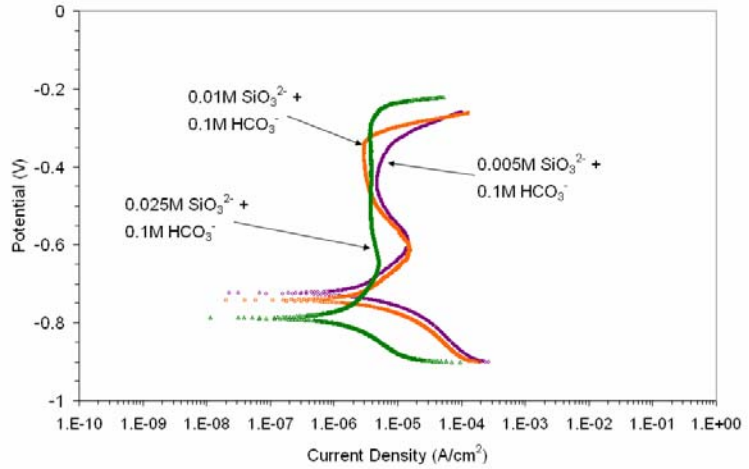

Figure 3.1.4. Potentiodynamic scans of AISI 4340 steel in deaerated, seawater solutions, with 0.1M $NaHCO_3$ and varying amounts of Na_2SiO_3 at 25°C.

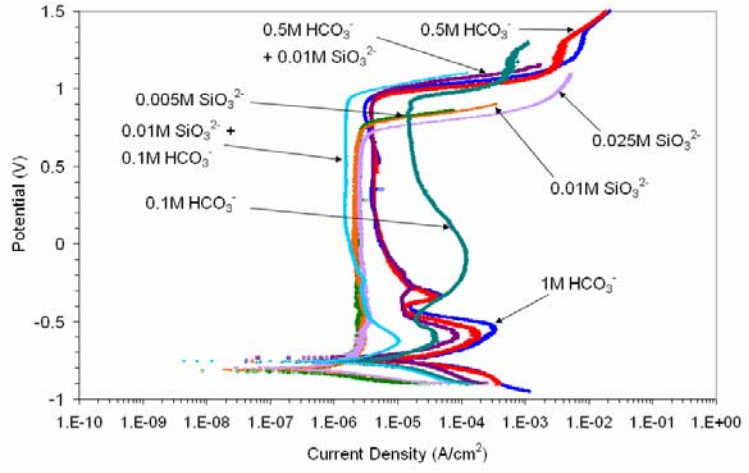

Figure 3.1.5. Potentiodynamic scans of AISI 4340 steel in deaerated HCO_3^- and/or SiO_3^{2-} solutions at 25°C.

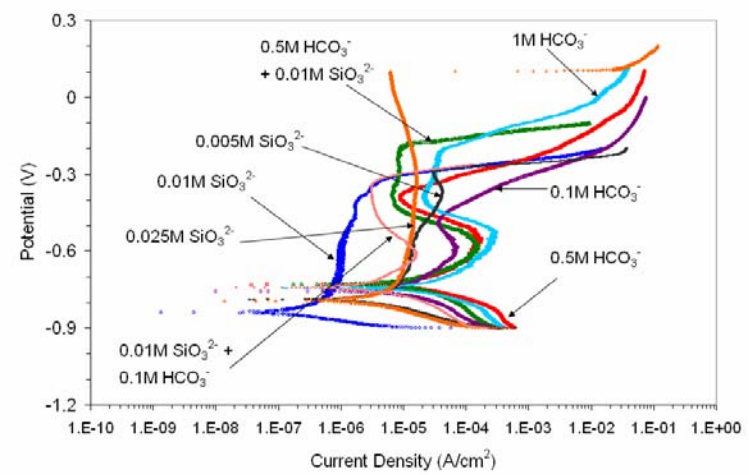

Figure 3.1.6. Potentiodynamic scans of AISI 4340 steel with different concentrations of HCO_3^- and/or SiO_3^{2-} ions in deaerated, simulated seawater (3.5 wt.% NaCl solution) at 25°C.

Electrochemical & Corrosion Rate Data – Tables & Graphs for 25°C

Tables 3.1.2 & 3.1.3, and Figures 3.1.7 – 3.1.10 show the electrochemical and corrosion rate data for 4340 steel in silicate and/or bicarbonate aqueous solutions at 25°C, both in pure water and simulated seawater.

Table 3.1.2 – Revised Electrochemical & Corrosion Rate Data for AISI 4340 Steel in Pure Water at 25°C

Ionic Concentration M (molarity)	Electrochemical & Corrosion Rate Data for AISI 4340 Steel in Pure Water at 25°C							
	Initial pH	Final pH	E_{corr} (mV)	I_{corr} (μA/cm²)	β_a (mV/decade)	β_c (mV/decade)	CR (μm/yr)	CR (mpy)
0.1M HCO_3^-	8.13	9.06	-0.761	7.7325	120	120	89.7996	3.5354
0.5M HCO_3^-	8.10	8.89	-0.749	25.7106	120	120	298.5846	11.7553
1M HCO_3^-	7.96	8.71	-0.753	39.5296	120	120	459.0681	18.0735
0.5M HCO_3^- + 0.005M SiO_3^{2-}	8.43	9.36	-0.739	12.6573	120	120	146.9928	5.7871
0.5M HCO_3^- + 0.01M SiO_3^{2-}	8.49	8.90	-0.734	11.0747	120	120	128.6140	5.0635
0.5M HCO_3^- + 0.025M SiO_3^{2-}	8.95	9.39	-0.740	14.8985	120	120	173.0202	6.8118
0.1M HCO_3^- + 0.005M SiO_3^{2-}	8.93	9.34	-0.739	4.6413	120	120	53.9002	2.1221
0.1M HCO_3^- + 0.01M SiO_3^{2-}	9.38	9.62	-0.758	3.7834	120	120	43.9373	1.7298
0.1M HCO_3^- + 0.025M SiO_3^{2-}	9.87	9.97	-0.787	2.6358	120	120	30.6101	1.2015
0.005M SiO_3^{2-}	11.03	11.17	-0.817	0.8705	120	120	10.1095	0.3980
0.01M SiO_3^{2-}	11.34	11.36	-0.812	1.2256	120	120	14.2332	0.5604
0.025M SiO_3^{2-}	11.78	11.74	-0.797	1.0892	120	120	12.6490	0.4980

Table 3.1.3 – Revised Electrochemical & Corrosion Rate Data for AISI 4340 Steel in Simulated Seawater at 25°C

Ionic Concentration M (molarity)	Electrochemical & Corrosion Rate Data for AISI 4340 Steel in Simulated Seawater at 25°C							
	Initial pH	Final pH	E_{corr} (mV)	I_{corr} (μA/cm²)	β_a (mV/decade)	β_c (mV/decade)	CR (μm/yr)	CR (mpy)
0.1M HCO_3^-	8.13	9.06	-0.755	13.9926	120	120	162.4998	6.3976
0.5M HCO_3^-	7.74	8.51	-0.732	26.6955	120	120	310.0222	12.2056

1M HCO_3^-	7.85	8.52	-0.746	29.1029	120	120	337.9800	13.3063
0.5M HCO_3^- + 0.005M SiO_3^{2-}	8.05	8.55	-0.720	22.1702	120	120	257.4689	10.1366
0.5M HCO_3^- + 0.01M SiO_3^{2-}	8.15	8.53	-0.727	18.9841	120	120	220.4678	8.6798
0.5M HCO_3^- + 0.025M SiO_3^{2-}	8.56	8.69	-0.738	10.7387	120	120	124.7118	4.9099
0.1M HCO_3^- + 0.005M SiO_3^{2-}	8.56	8.70	-0.725	5.0058	120	120	58.1333	6.2869
0.1M HCO_3^- + 0.01M SiO_3^{2-}	8.86	9.05	-0.743	4.8267	120	120	56.0534	2.2068
0.1M HCO_3^- + 0.025M SiO_3^{2-}	9.39	9.45	-0.787	1.7705	120	120	20.5618	0.8095
0.005M SiO_3^{2-}	11.09	10.98	-0.789	5.4574	120	120	63.3788	2.4952
0.01M SiO_3^{2-}	11.12	11.10	-0.839	0.4499	120	120	5.2253	0.2057
0.025M SiO_3^{2-}	11.48	11.46	-0.793	4.8423	120	120	56.2347	2.2140

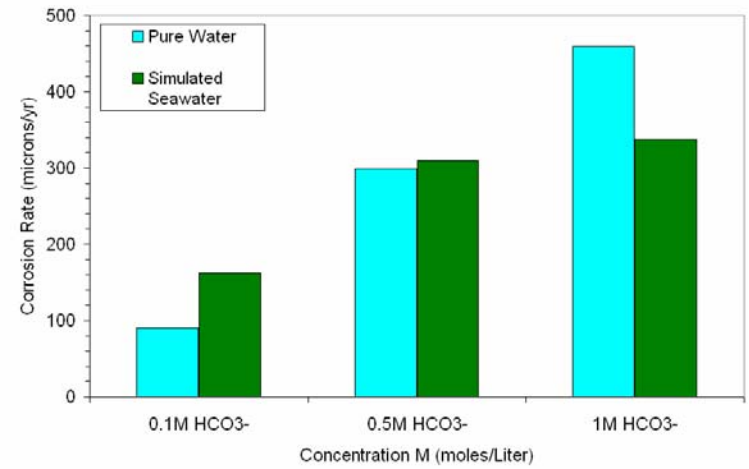

Figure 3.1.7. Comparison of the corrosion rates of 4340 steel at 25°C in deaerated, HCO_3^- solutions, with and without 3.5 wt.% NaCl.

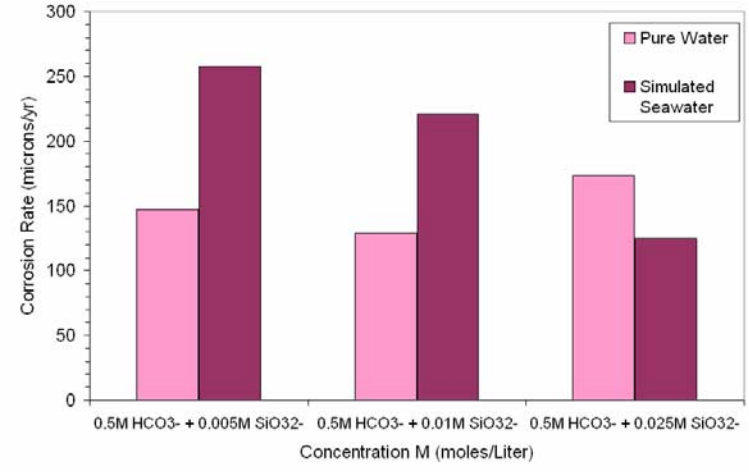

Figure 3.1.8. Comparison of the corrosion rates of 4340 steel at 25°C in deaerated, silicate solutions with 0.5M HCO_3^-, with and without 3.5 wt.% NaCl.

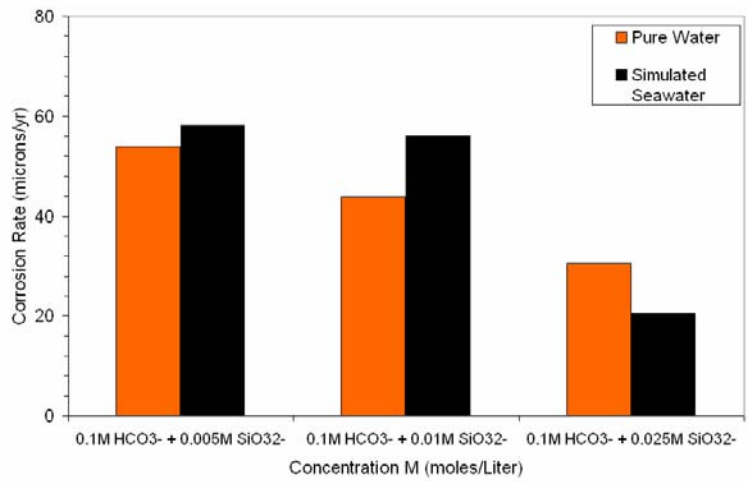

Figure 3.1.9. Comparison of the corrosion rates of 4340 steel at 25°C in deaerated, silicate solutions with 0.5M HCO_3^-, with and without 3.5 wt.% NaCl.

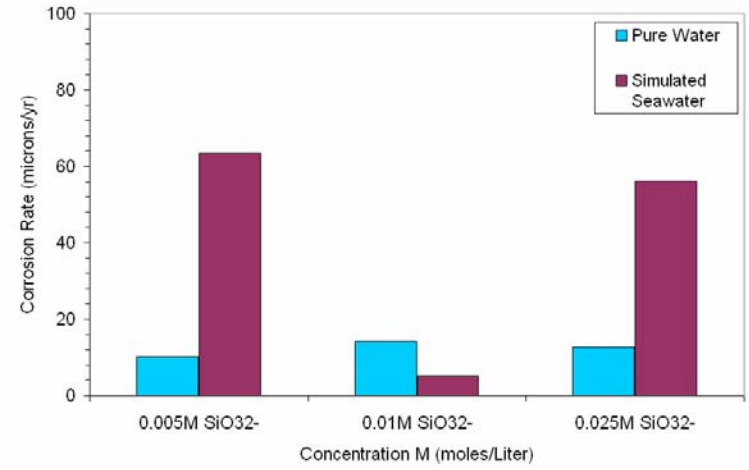

Figure 3.1.10. Comparison of the corrosion rates of 4340 steel at 25°C in deaerated, SiO_3^{2-} solutions, with and without 3.5 wt.% NaCl.

Electrochemical Polarization & Passivity – 45°C

In this section, we present new results of the experiments performed at 45°C. Figures 3.1.11 – 3.1.22 show representative potentiodynamic scans of AISI 4340 steel using sodium bicarbonate ($NaHCO_3$) and/or sodium silicate (Na_2SiO_3), in pure water and simulated seawater (3.5% NaCl). Tables 3.1.3 and 3.1.4 show the electrochemical and corrosion rate data from these figures.

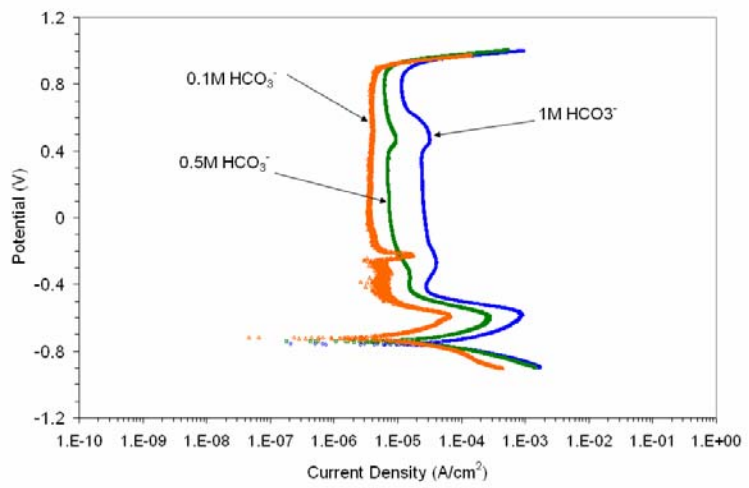

Figure 3.1.11. Potentiodynamic scans of AISI 4340 steel in deaerated, bicarbonate solutions at 45°C.

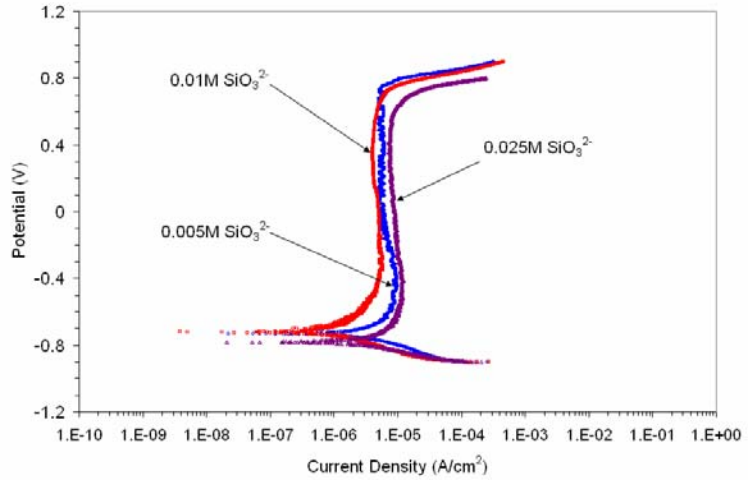

Figure 3.1.12. Potentiodynamic scans of AISI 4340 steel in deaerated, silicate solutions at 45°C.

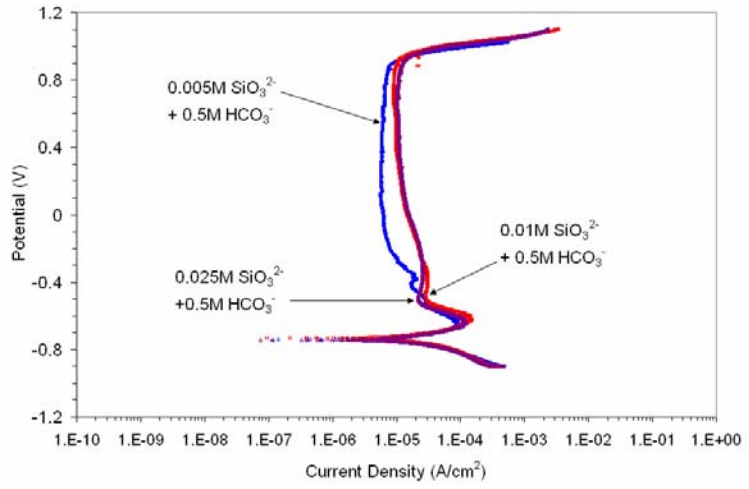

Figure 3.1.13. Potentiodynamic scans of AISI 4340 steel in deaerated, pure water solutions with 0.5M $NaHCO_3$ and varying amounts of Na_2SiO_3 at 45°C.

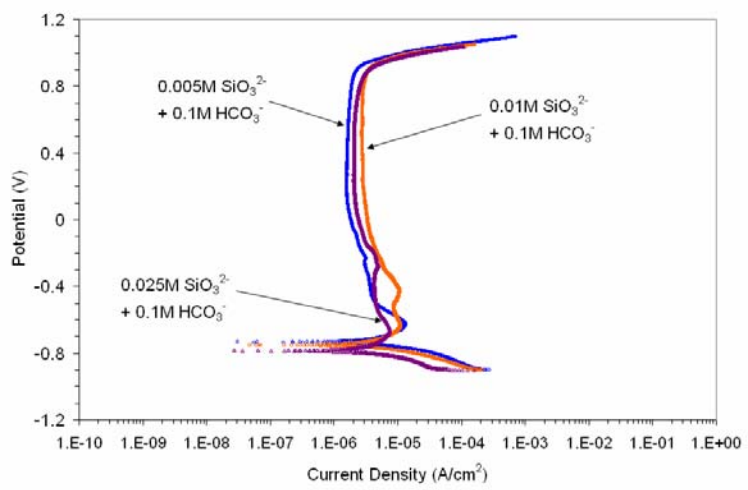

Figure 3.1.14. Potentiodynamic scans of AISI 4340 steel in deaerated, pure water solutions with 0.1M $NaHCO_3$ and varying amounts of Na_2SiO_3 at 45°C.

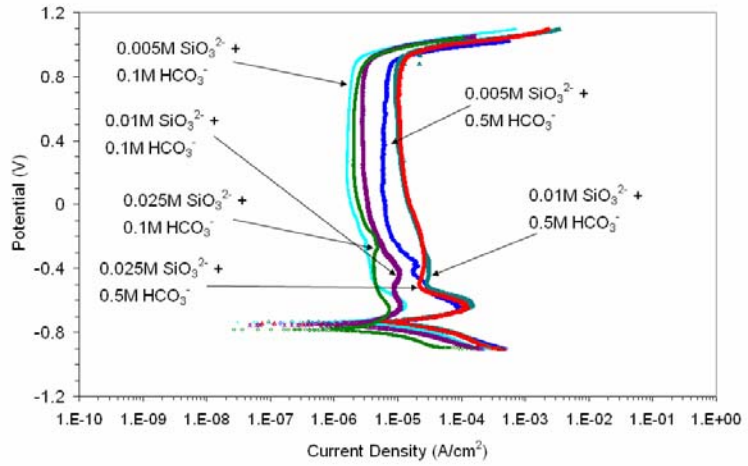

Figure 3.1.15. Potentiodynamic scans of AISI 4340 steel in deaerated, pure water solutions with 0.1M & 0.5M $NaHCO_3$, and varying amounts of Na_2SiO_3 at 45°C.

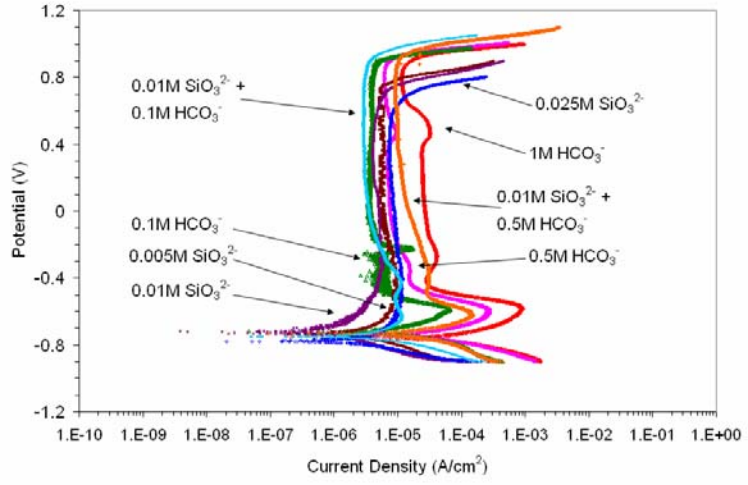

Figure 3.1.16. Potentiodynamic scans of AISI 4340 steel in deaerated, pure water solutions containing various concentrations of $NaHCO_3$ and/or Na_2SiO_3 at 45°C.

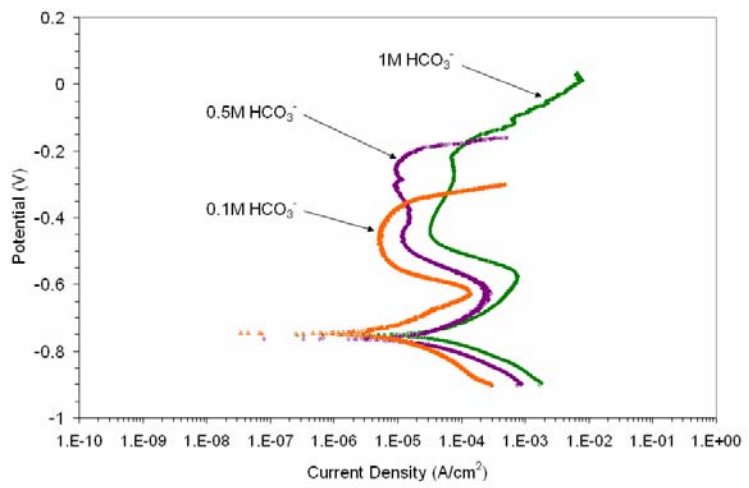

Figure 3.1.17. Potentiodynamic scans of AISI 4340 steel in deaerated, simulated seawater containing various amounts of $NaHCO_3$ at 45°C.

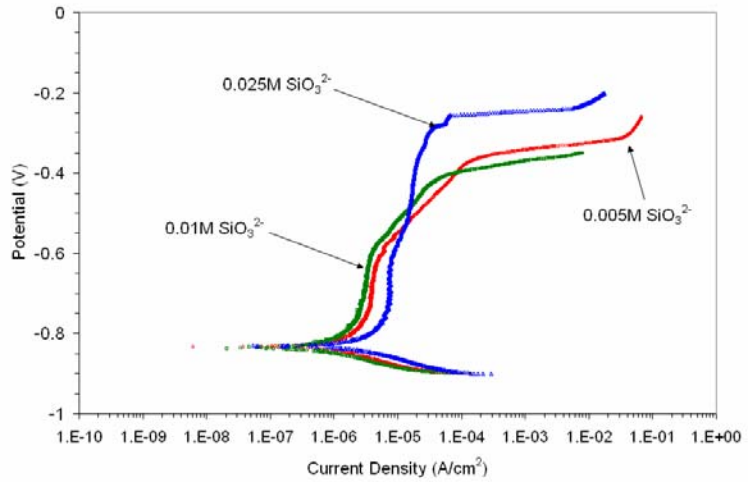

Figure 3.1.18. Potentiodynamic scans of AISI 4340 steel in deaerated, simulated seawater containing various amounts of Na_2SiO_3 at 45°C.

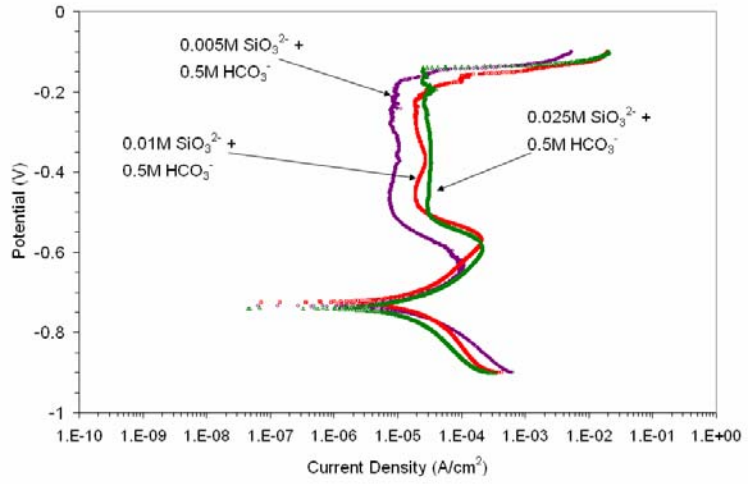

Figure 3.1.19. Potentiodynamic scans of AISI 4340 steel in deaerated, simulated seawater containing 0.5M $NaHCO_3$ and various amounts of Na_2SiO_3 at 45°C.

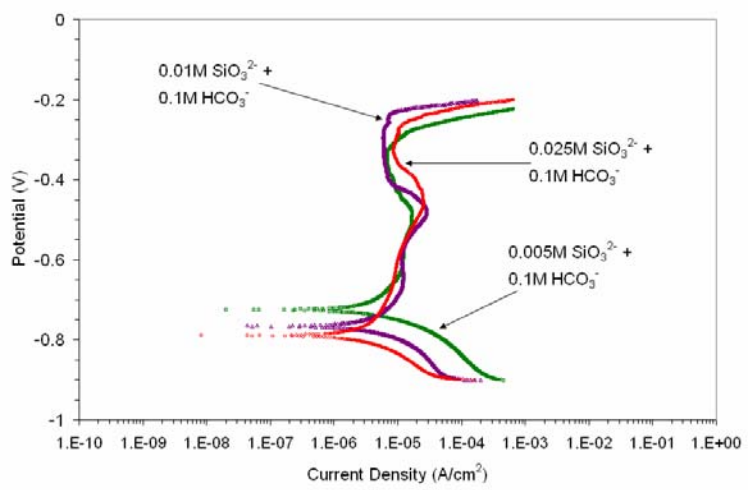

Figure 3.1.20. Potentiodynamic scans of AISI 4340 steel in deaerated, simulated seawater containing 0.1M $NaHCO_3$ and various amounts of Na_2SiO_3 at 45°C.

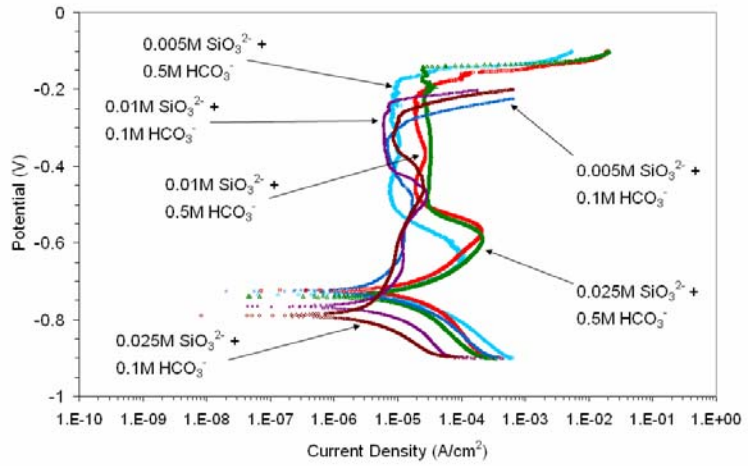

Figure 3.1.21. Potentiodynamic scans of AISI 4340 steel in deaerated, simulated seawater containing 0.1M & 0.5M $NaHCO_3$ and various amounts of Na_2SiO_3 at 45°C.

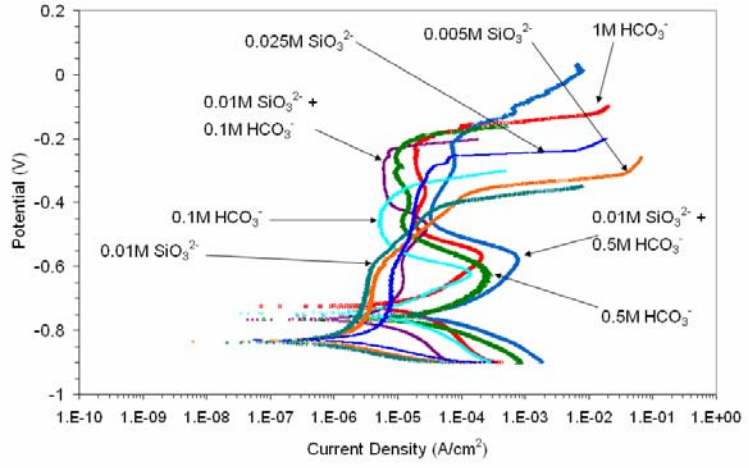

Figure 3.1.22. Potentiodynamic scans of AISI 4340 steel in deaerated, seawater solutions containing various concentrations of $NaHCO_3$ and/or Na_2SiO_3 at 45°C.

Electrochemical & Corrosion Rate Data – Tables & Graphs for 45°C

Tables 3.1.4 & 3.1.5, along with Figures 3.1.23 – 3.1.26, give a complete perspective of the effects of sodium silicate and/or sodium bicarbonate on 4340 steel at 45°C, both in pure water and simulated seawater.

Table 3.1.4 – Electrochemical & Corrosion Rate Data for AISI 4340 Steel in Pure Water at 45°C

Ionic Concentration M (molarity)	Electrochemical & Corrosion Rate Data for AISI 4340 Steel in Pure Water at 45°C							
	Initial pH	Final pH	E_{corr} (mV)	I_{corr} ($\mu A/cm^2$)	β_a (mV/decade)	β_c (mV/decade)	CR (μm/yr)	CR (mpy)
0.1M HCO_3^-	8.28	9.47	-0.720	11.4395	120	120	132.8499	5.2303
0.5M HCO_3^-	8.22	9.36	-0.744	42.0426	120	120	488.2521	19.2225
1M HCO_3^-	8.15	9.22	-0.760	90.0014	120	120	1045.2111	41.15
0.5M HCO_3^- + 0.005M SiO_3^{2-}	8.42	9.54	-0.745	19.9205	120	120	231.3420	9.1080
0.5M HCO_3^- + 0.01M SiO_3^{2-}	8.51	9.15	-0.734	23.4833	120	120	272.7178	10.7369
0.5M HCO_3^- + 0.025M SiO_3^{2-}	8.98	9.13	-0.741	21.4633	120	120	249.2592	9.8134
0.1M HCO_3^- + 0.005M SiO_3^{2-}	9.10	9.47	-0.735	6.2295	120	120	72.3452	2.8482
0.1M HCO_3^- + 0.01M SiO_3^{2-}	9.41	9.79	-0.752	5.4617	120	120	63.4279	2.4972
0.1M HCO_3^- + 0.025M SiO_3^{2-}	9.92	10.01	-0.784	4.8209	120	120	55.9860	2.2042
0.005M SiO_3^{2-}	11.13	10.84	-0.735	3.1772	120	120	36.8975	1.4527
0.01M SiO_3^{2-}	11.43	11.33	-0.720	1.0097	120	120	11.7258	0.4616
0.025M SiO_3^{2-}	11.80	11.57	-0.781	2.9829	120	120	34.6413	1.3638

Table 3.1.5 – Electrochemical & Corrosion Rate Data for AISI 4340 Steel in Seawater at 45°C

Ionic Concentration M (molarity)	Electrochemical & Corrosion Rate Data for AISI 4340 Steel in Simulated Seawater at 45°C							
	Initial pH	Final pH	E_{corr} (mV)	I_{corr} ($\mu A/cm^2$)	β_a (mV/decade)	β_c (mV/decade)	CR (μm/yr)	CR (mpy)
0.1M HCO_3^-	8.02	9.14	-0.745	11.0283	120	120	128.075	5.0423
0.5M HCO_3^-	7.81	9.10	-0.763	38.0931	120	120	442.3863	17.4168
1M HCO_3^-	7.84	8.83	-0.753	73.3679	120	120	852.0416	33.5449
0.5M HCO_3^- + 0.005M SiO_3^{2-}	8.07	9.06	-0.734	19.4694	120	120	226.1031	8.9017
0.5M HCO_3^- + 0.01M SiO_3^{2-}	8.25	8.50	-0.725	18.6005	120	120	216.0128	8.5044
0.5M HCO_3^- + 0.025M SiO_3^{2-}	8.52	8.65	-0.739	14.7835	120	120	171.6849	6.7592
0.1M HCO_3^- + 0.005M SiO_3^{2-}	8.63	8.95	-0.784	6.7117	120	120	77.9445	3.0687
0.1M HCO_3^- + 0.01M SiO_3^{2-}	8.88	9.21	-0.765	6.0024	120	120	69.7080	2.7444
0.1M HCO_3^- + 0.025M SiO_3^{2-}	9.42	9.53	-0.790	4.3061	120	120	50.0076	1.9688
0.005M SiO_3^{2-}	10.98	10.64	-0.835	2.3641	120	120	27.4549	1.0809
0.01M SiO_3^{2-}	10.97	10.67	-0.837	1.6862	120	120	19.5822	0.7710
0.025M SiO_3^{2-}	11.50	11.14	-0.831	4.8285	120	120	56.0752	2.2077

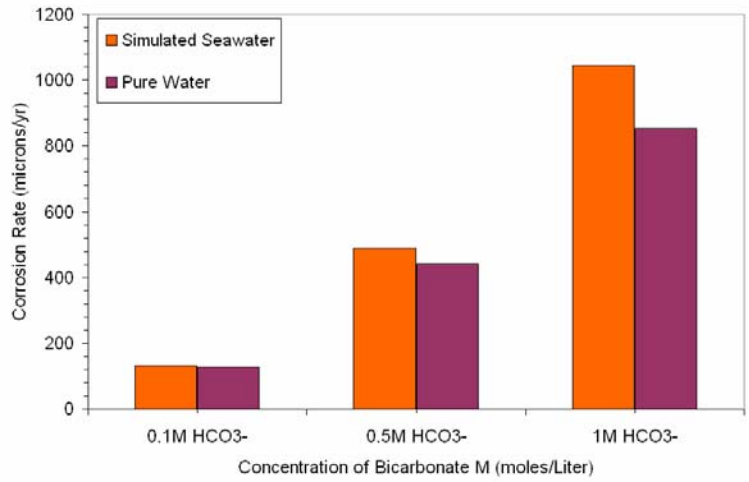

Figure 3.1.23. Comparison of the corrosion rates of 4340 steel at 45°C in deaerated, HCO_3^- solutions with and without 3.5 wt.% NaCl.

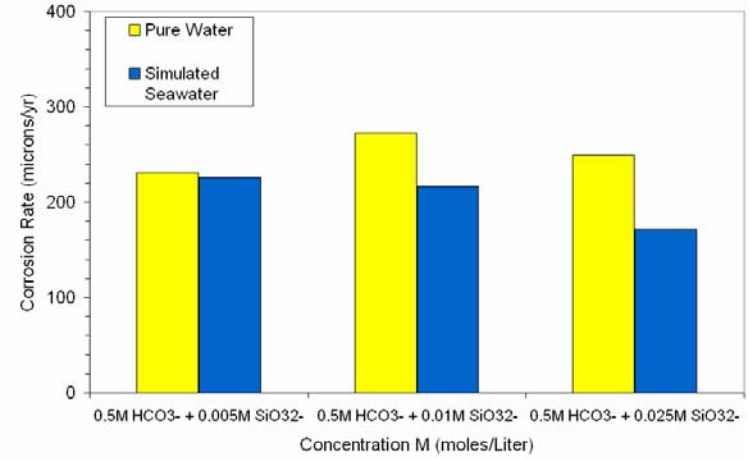

Figure 3.1.24. Comparison of the corrosion rates of 4340 steel at 45°C in deaerated, silicate solutions with 0.5M HCO_3^-, with and without 3.5 wt.% NaCl.

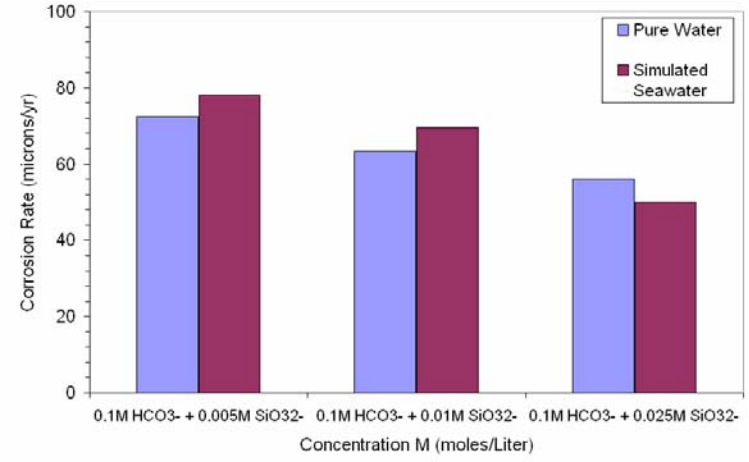

Figure 3.1.25. Comparison of the corrosion rates of 4340 steel at 45°C in deaerated, silicate solutions with 0.1M HCO_3^-, with and without 3.5 wt.% NaCl.

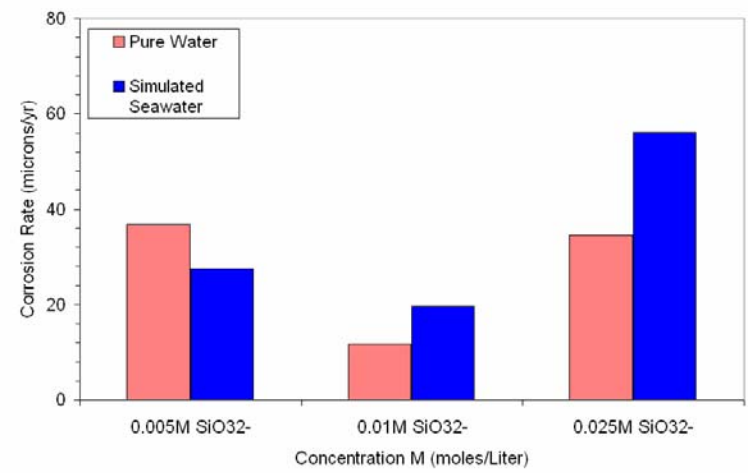

Figure 3.1.26. Comparison of the corrosion rates of 4340 steel at 45°C in deaerated, SiO_3^{2-} solutions with and without 3.5 wt.% NaCl.

Comparison of Corrosion Rates at 25°C and 45°C in Pure Water and Simulated Seawater

In this section, we compare results derived from the previous sections. Figures 3.1.27 – 3.1.34 show additional bar graphs for 4340 steel in silicate and/or bicarbonate solutions at 25°C & 45°C, comparing corrosion rates in pure water versus simulated seawater.

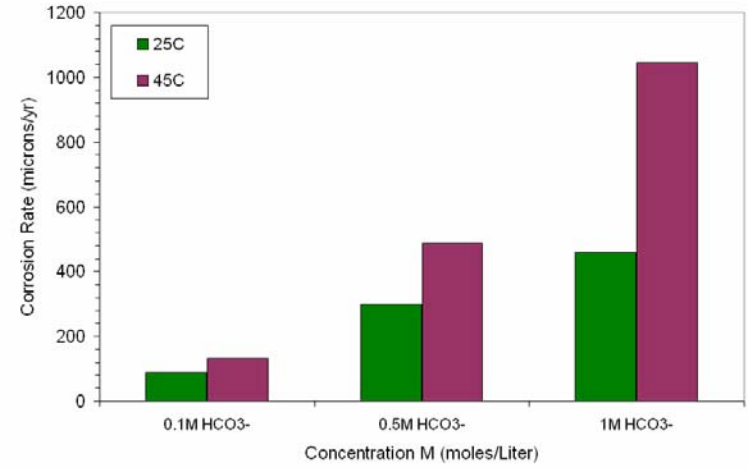

Figure 3.1.27. Comparison of the corrosion rates of 4340 steel at 25°C & 45°C in deaerated, HCO_3^- solutions without 3.5 wt.% NaCl – i.e. pure water only.

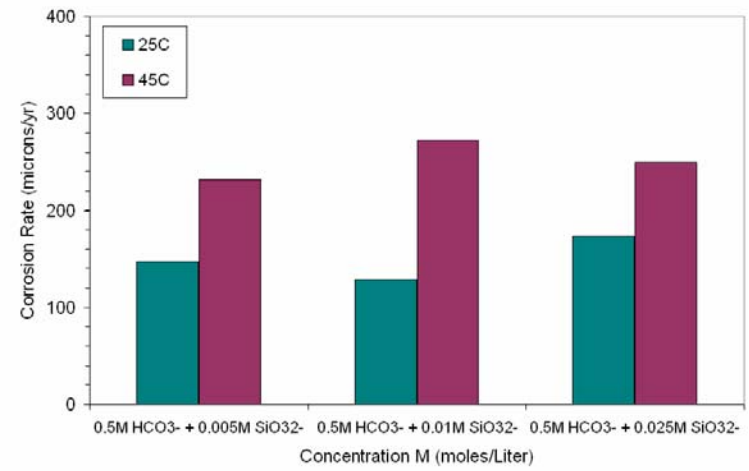

Figure 3.1.28. Comparison of the corrosion rates of 4340 steel at 25°C & 45°C in deaerated, silicate solutions with 0.5M HCO_3^-, without 3.5 wt.% NaCl – i.e. pure water only.

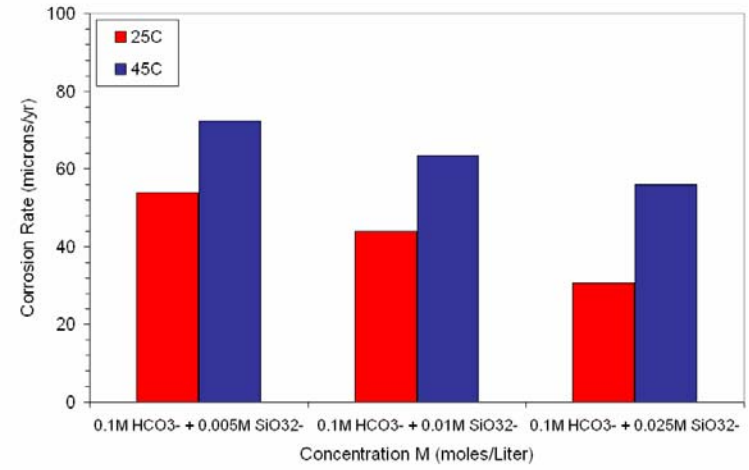

Figure 3.1.29. Comparison of the corrosion rates of 4340 steel at 25°C & 45°C in deaerated, silicate solutions with 0.1M HCO_3^-, without 3.5 wt.% NaCl – i.e. pure water only.

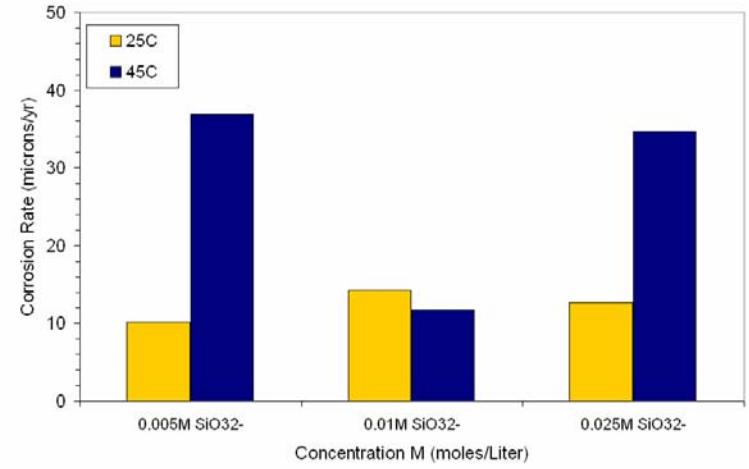

Figure 3.1.30. Comparison of the corrosion rates of 4340 steel at 25°C & 45°C in deaerated, SiO_3^{2-} solutions without 3.5 wt.% NaCl – i.e. pure water only.

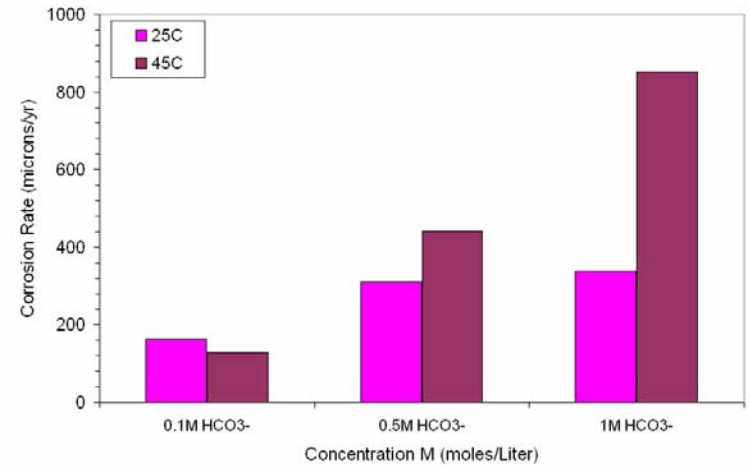

Figure 3.1.31. Comparison of the corrosion rates of 4340 steel at 25°C & 45°C in deaerated, HCO_3^- solutions with 3.5 wt.% NaCl – i.e. simulated seawater only.

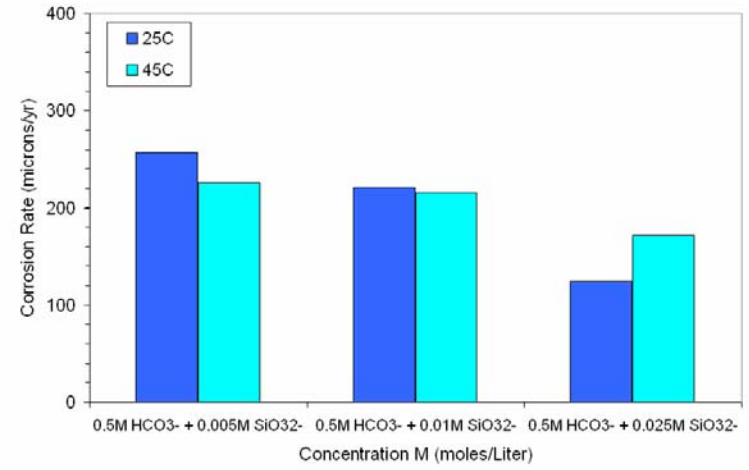

Figure 3.1.32. Comparison of the corrosion rates of 4340 steel at 25°C & 45°C in deaerated, silicate solutions with 0.5M HCO_3^-, with 3.5 wt.% NaCl – i.e. simulated seawater only.

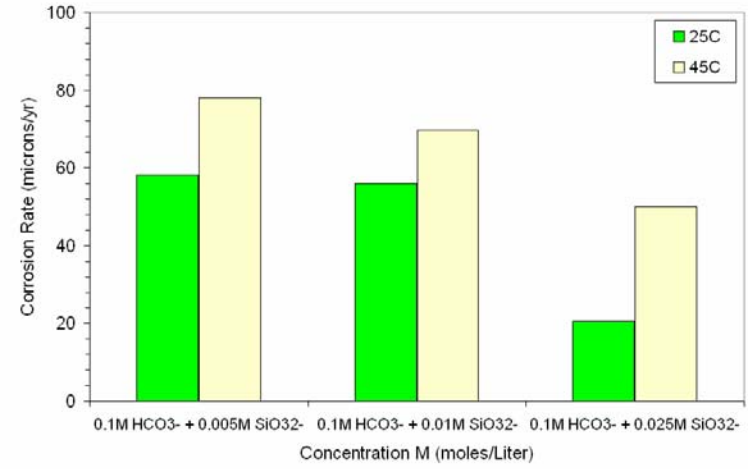

Figure 3.1.33. Comparison of the corrosion rates of 4340 steel at 25°C & 45°C in deaerated, silicate solutions with 0.1M HCO_3^-, with 3.5 wt.% NaCl – i.e. simulated seawater only.

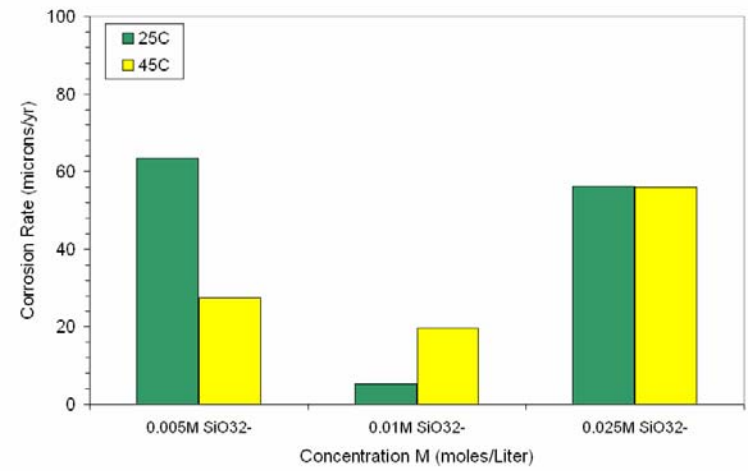

Figure 3.1.34. Comparison of the corrosion rates of 4340 steel at 25°C & 45°C in deaerated, SiO_3^{2-} solutions with 3.5 wt.% NaCl – i.e. simulated seawater only.

3.1.4 Discussion

Electrochemical Behavior of AISI 4340 Steel in Pure Water & Simulated Seawater

Representative potentiodynamic scans of 4340 steel in sodium silicate and/or sodium bicarbonate in pure water and simulated seawater at 25°C are shown in Figures 3.1.1 – 3.1.4. Figures 3.1.5 and 3.1.6 were revised to include [0.01M Na_2SiO_3 + 0.1M $NaHCO_3$] scans for reference. Additionally, Figures 3.1.11 – 3.1.22 show representative potentiodynamic scans of 4340 steel in sodium silicate and/or sodium bicarbonate in pure water and simulated seawater at 45°C. These figures show similar trends and behaviors, both between the two temperatures and within each chemical composition. Therefore, they will be discussed concurrently.

For all potentiodynamic scans presented, the passivity obtained by the steel in solutions without chlorides is much greater than the passivity obtained in the presence of chlorides. This is evident by comparing Figures 3.1.1 & 3.1.2 to 3.1.3 & 3.1.4 (for 25°C) and Figures 3.1.11 – 3.1.15 to 3.1.17 – 3.1.22 (for 45°C). Figures 3.1.5 & 3.1.6 (25°C) and Figures 3.1.16 & 3.1.22 (45°C) provide overall comparisons as well. In these potentiodynamic scans, not only is the amount of passivity obtained much larger without chlorides (~ 1000 mV to 1200 mV), but the amount of current required to obtain passivity is less by (approximately) a factor of 10. This is due to the deleterious effects of chlorides in solution, which is well known to induce pitting in the steel.[7] Therefore, more current (and more current density) is required to maintain a passive film over the steel's surface. However, that passive film is much smaller (in terms of its overall voltage range) than the films formed in the same solutions without chlorides present. Figure 3.1.5 illustrates this difference very well. Another aspect is in the inherent stability of the film formed. For higher concentrations of bicarbonate, silicate, or both, the passive film formed on the steel's surface is much more stable at higher concentrations than at lower ones. For example, less bicarbonate is required to obtain passivity when sodium silicate is added and its concentration is varied. This is evident in Figure 3.1.15, which shows a composite graph of Figures 3.1.13 & 3.1.14 together, as compared to Figure 3.1.11, which shows just bicarbonate in pure water by itself. From observation, it can be understood that a decrease in the bicarbonate concentration by 80% decreases the amount of current required to transition from oxidation to passivity (Figures 3.1.2 & 3.1.14). Also, an increase in the concentration of SiO_3^{2-} ions lowers the open circuit potential (E_{corr}), resulting in a lower corrosion rate. This also happens to be the case in the presence of simulated seawater (3.5 wt.% NaCl solution).

In simulated seawater, based on experimental observations, a certain amount of dissolved sodium silicate overrides the deleterious effects of Cl^- ions and/or HCO_3^- ions, resulting in a lower corrosion rate as the concentration of sodium silicate increases in solution. This is most likely due to the amorphous structure of

silica (SiO_2) covering the specimen's surface during potentiodynamic polarization.[8] However, there also seems to be a maximum amount required to minimize the corrosion rate when bicarbonate is not present. This can be seen in Tables 3.1.2 – 3.1.5, with concentrations of silicate ions in both pure water and seawater. When $NaHCO_3$ is alone in solution, it dissociates and combines with iron to make $Fe(HCO_3)_2$ and then to $FeCO_3$.[9] This transformation is accompanied by shrinkage and formation of a porous, non-adherent and non-protective layer that allow chloride ions to penetrate and help continue the pitting process.[9] However, if Na_2SiO_3 is added to the solution, the SiO_3^{2-} ions dissociate and form SiO_2, which covers the surface of the steel like a coating or film, decreasing the corrosion rate. This is most likely due to the strong, amorphous bonds of the silica, giving the film a "honeycomb-like" structure.[8] This phenomenon was reported on the surface of "As-Inflated" *Swellex Mn-24* Rock Bolt steel, potentiostatically tested in 1X Yucca Mountain water at -530 mV at 25°C for two hours.[10] These observations are important to consider for a possible corrosion inhibitor, as the cost for the chemicals used in the inhibitor(s) is an important factor in the preparation of the rock bolts.

Other similarities exist, such as the initial and final pH readings for solutions containing different concentrations of bicarbonate or silicate ions. In both pure water and simulated seawater, the initial and final pH readings for bicarbonate decrease as the concentration of bicarbonate ions increases. Also, the corrosion rates increase as the bicarbonate concentration increases. This makes sense because the more bicarbonate ions exist in solution, more carbonic acid (H_2CO_3) is formed. This increases the solution's acidity, which allows more CO_2 gas to form, due to the dissociation of HCO_3^-. This dissolved CO_2 gas pits the steel by attaching to the steel surface as small gas bubbles. These bubbles then induce a crevice around themselves, which develops into a pit.[9] These surface products were discussed extensively in the previous quarterly report.[11]

Tables 3.1.2 & 3.1.3 show the electrochemical and corrosion rate data for all experiments run at 25°C, including the data reported in the last quarterly report. Figures 3.1.7 – 3.1.10 show bar graphs comparing the corrosion rate data presented in Tables 3.1.2 & 3.1.3, in pure water versus simulated seawater. Tables 3.1.4 & 3.1.5 show the electrochemical and corrosion rate data for experiments run at 45°C. Figures 3.1.23 – 3.1.26 show bar graphs comparing the corrosion rate data shown in Tables 3.1.4 & 3.1.5, in pure water vs. simulated seawater. Additionally, Figures 3.1.27 – 3.1.34 compare the corrosion rates for 4340 steel at 25°C versus 45°C, for both pure water and seawater, respectively. For the most part, the corrosion rates follow systematic patterns. In general, corrosion rates increase as the concentration of bicarbonate increases, and decrease as the concentration of silicate increases. This pattern of behavior also pertains to rates where the amount of bicarbonate is fixed and the amount of silicates is varied (increased or decreased). These trends follow for both pure water solutions and simulated seawater solutions. However, there is some abnormal pattern behavior observed, such as in Figure 3.1.30 or Figure 3.1.34, which show that 0.01M Na_2SiO_3 is lower (mostly) than the other two silicate concentrations for both 25°C and 45°C, in both pure water and seawater. Any abnormalities could be attributed to a small sample size (2 to 3 experiments done per set). However, due to the enormous amount of work involved in obtaining the results over a wide (i.e. – projected) temperature range (25°C – 90°C), two to three experiments per concentration seems reasonable for overall projected trends and behaviors.

3.1.5 Summary

The passivity effects of sodium silicate and sodium bicarbonate have been investigated by potentiodynamic polarization using AISI 4340 steel at 25°C & 45°C. The results from these tests, as well as other tests at higher temperatures, will be used to help determine a corrosion inhibitor for 4340 steel. Results show that when sodium silicate is used solely as an inhibitor for 4340 steel, the steel exhibits a large passive region, somewhat similar to Hastelloy® C-22.[12] Although sodium bicarbonate alone gives a large amount of passivity for this high-strength steel, the corrosion rates are much higher than those obtained from using sodium silicate. Also, sodium bicarbonate in simulated seawater induces pitting beyond the passive regions due to dissolved carbon dioxide bubbles attached to the surface of the steel. These bubbles enable the carbon dioxide to continue to pit the surface of the steel. However, when sodium silicate is used in pure water and simulated seawater, the silicate ions are able to adhere to the surface of the steel and prevent diffusion of chlorides or other ions from reaching the surface due to its amorphous structure.[8] This allows

4340 steel to obtain a very large passive region, which further increases the possibility of using this high-strength steel in structural applications inside the Yucca Mountain repository.

3.1.6 References

1. M. Mohorich, Scientific Notebook #UCCSN-UNR-095, vol. 1 (September 2005), p. 6.
2. D. Chandra and J. Daemen, *Quarterly Technical Report #6 – Sub-surface Corrosion Research on Rock Bolt System, Perforated SS Sheets and Steel Sets for the Yucca Mountain Repository,* United States Department of Energy – Office of Civilian Defense Radioactive Waste Management: Yucca Mountain Project, Metallurgical & Materials Engineering, University of Nevada-Reno, January 2006.
3. ASTM G-59, Annual Book of ASTM standards, Vol. 03.02, 1989.
4. ASTM G-102, Annual Book of ASTM standards, Vol. 03.02, 1989.
5. Yilmaz, D. Chandra, and R.B. Rebak, *Corrosion Behavior of Carbon Steel Rock Bolt in Simulated Yucca Mountain Ground Waters*, Metallurgical and Materials Transactions A, vol. 36A (2005), pp. 1097 – 1105.
6. F. Mansfeld, *Advances in Corrosion Science and Technology, vol. 6,* M.G. Fontana and R.W. Staehle, eds., Plenum Press, New York, NY, 1976, p. 180.
7. D.A. Jones, *Principles and Prevention of Corrosion*, 2nd ed., Prentice Hall, Upper Saddle River, NJ, 1996, p. 200.
8. L. Lehrman & H.L. Shuldener, *Action of Sodium Silicate as a Corrosion Inhibitor in Water Piping*, Journal of Industrial and Engineering Chemistry, 44 (1952), pp. 1765 – 1769.
9. Z. Xia, K.-C. Chou and Z. Szklarska-Smialowska, *Pitting Corrosion of Carbon Steel in CO_2-Containing NaCl Brine,* Corrosion, vol. 45 [8] (1989), pp. 636 – 642.
10. D. Chandra and J. Daemen, *Quarterly Technical Report #11 – Sub-surface Corrosion Research on Rock Bolt System, Perforated SS Sheets and Steel Sets for the Yucca Mountain Repository,* United States Department of Energy – Office of Civilian Defense Radioactive Waste Management: Yucca Mountain Project, Metallurgical & Materials Engineering, University of Nevada-Reno, April 2007.
11. D. Chandra and J. Daemen, *Quarterly Technical Report #12 – Sub-surface Corrosion Research on Rock Bolt System, Perforated SS Sheets and Steel Sets for the Yucca Mountain Repository,* United States Department of Energy – Office of Civilian Defense Radioactive Waste Management: Yucca Mountain Project, Metallurgical & Materials Engineering, University of Nevada-Reno, July 2007.
12. M.S. Rahman, *Electrochemical Behavior of Alloy 22 and Friction Type Rock Bolt,* Ph.D. Dissertation, Univ. of Nevada-Reno, University Press, December 2006, p. 45.